Supporting information for:

Electron-rich biochar enhanced Z-scheme heterojunctioned bismuth tungstate/ bismuth oxyiodide removing tetracycline

Fuyan Kang[a,#], Xiaona Jiang[a,#], Yao Wang[a], Juanna Ren,[b,c] Ben Bin Xu,[b] Guoyang Gao[a], Zhanhua Huang[a,*], Zhanhu Guo[b,*]

[a] Key Laboratory of Bio-based Material Science and Technology, Ministry of Education, Material Science and Engineering College, Northeast Forestry University, Harbin 150040, Heilongjiang, China

[b] Mechanical and Construction Engineering, Faculty of Engineering and Environment, Northumbria University, Newcastle Upon Tyne, NE1 8ST, UK

[c] College of Materials Science and Engineering, Taiyuan University of Science and Technology, Taiyuan, 030024, China

[1]These authors contributed equally.

*****Corresponding authors.

E-mail addresses: huangzh1975@163.com (Z. Huang), zhanhu.guo@northumbria.ac.uk (Z. Guo).

Experimental Sections

Characterization.

The morphologies of the synthesized samples were characterized by field emission scanning electron microscopy (FE-SEM) (S-3400, Hitachi, Japan), transmission electron microscopy (TEM) and high-resolution transmission electron microscopy (HRTEM) (JEM-2100, JEOL, Japan) at an accelerating voltage of 200 kV. X-ray diffraction (XRD) (D/max-2200VPC, Rigaku, Japan) was performed to determine the crystal structures of materials under Cu Kα radiation (40 kV, 30 mA) with a scanning range of 10–90° at a speed of 5° min^{-1}. Surface element chemical compositions were analyzed by X-ray photoelectron spectroscopy (XPS) (PHI5700, Thermo Electron Corporation, USA) using non-monochromatic Al X-rays as the primary excitation. N_2 adsorption–desorption isotherms and pore-size distributions were studied using a nitrogen adsorption analyzer (ASAP2020, Micromeritics, USA). UV-vis diffuse reflectance spectra (UV-vis DRS) of samples were recorded using a double-beam ultraviolet–visible spectrophotometer (TU-1901, Beijing General Instrument Co., Ltd., China) using $BaSO_4$ as a reference in the scan range of 200–800 nm. UV-vis spectra were acquired using a UV-vis spectrophotometer (TU-1900, Beijing General Instrument Co., Ltd., China). Photoluminescence (PL) spectra of solid powders were measured using a Cary Eclipse fluorescence spectrophotometer (Agilent Technologies, Australia). Fourier transform infrared (FT-IR) spectra were obtained using a Fourier-transform infrared spectrometer (iS10, Nicolet, USA) scanning from 4000–400 cm□1 with a resolution of 4 cm^{-1}. The glass tube was then inserted into the ESR cavity and

was irradiated under a 300 W Xenon lamp, and the spectra were recorded at selected times. Electron spin resonance (ESR) spectra were recorded at room temperature using a Bruker A200 EPR spectrometer with center field at 3398 G and X-band microwave frequency of 9.45 GHz. The intermediates formed during the photocatalytic reaction of TC over BCs-Bi_2WO_6 was examined using a liquid chromatography-mass spectrometry (LCMS) coupled with a mass spectrometer (Waters Micromass Q-TOFMicro). Electrochemical impedance spectra (EIS) and photocurrent transient response (I-t) were measured in a three-electrode system on an electrochemical workstation (CHI660E, Shanghai, China). Na_2SO_4 aqueous solution (0.50 M) was used as the electrolyte. A Pt plate and Ag/AgCl electrode were used as the counter and reference electrode, respectively, while working electrodes were prepared by spreading a slurry of the as-prepared photocatalyst onto fluorine-doped tin oxide (FTO) glass.

Preparation of Bi_2WO_6

0.5 mmol $Bi(NO_3)_3 \cdot 5H_2O$ and 0.5 mmol $Na_2WO_4 \cdot 2H_2O$ were weighed and dispersed in 30 mL of ethylene glycol solution and stirring for 30min. The stirred solution was transferred to a hydrothermal reactor and reacted at 140 ℃ for 14 h. The reacted precipitate is collected and washed and dried.

Synthesis of BiOI

2 mmol of $Bi(NO_3)_3 \cdot 5H_2O$ and 2 mmol of KI were weighed and dispersed in 30 mL of ethylene glycol. Meanwhile, the dispersed solution was stirred for 30 min. The stirred solution was transferred to a hydrothermal reactor at 140 ℃ and reacted for 14 h. The reacted precipitate is collected and washed and dried.

Synthesis of BC

BCs were prepared using high-temperature carbonization and alkaline activation methods. Firstly, wash, dry, and crush the corncob to obtain corncob powder. Then pre carbonize the corn cob powder at 450 °C for 2 h (with a heating rate of 5 °C·min^{-1}) and continuously introduce N_2 protection to obtain pre carbonized corn cob charcoal. Then mix pre carbonized corn cob charcoal and KOH in a mass ratio of 1:4, and carbonize at 900 °C for 1 h (heating rate of 5 °C·min^{-1}). Finally, wash and dry the above samples with concentrated H_2SO_4 to obtain BCs.

Adsorption model

Adsorption kinetics: using the pseudo-first-order model (Eq(S1)) and the pseudo-second-order model (Eq(S2)) to predict the adsorption mechanism of tetracycline (TC) on the catalyst surface. The procedure of the adsorption kinetics experiment was as follows: Take 10 mg of catalyst and added it to 100 mL of TC (50 mg L^{-1}), and stirred at 298 K. The decisive step model of catalyst adsorption of TC was fitted by the Intra-particle diffusion model (Eq(S3))

pseudo-first-order model

$$q_t = q_e(1 - e^{k_1 t}) \quad \text{(S1)}$$

Where qt is the adsorption capacity of TC at t (min), k_1 (min^{-1}) is the rate constant of pseudo-first-order model.

pseudo-second-order model

$$q_t = \frac{q_e^2 K_2 t}{1 + q_e K_2 t} \quad \text{(S2)}$$

Where k_2 is the rate constant of the pseudo-second-order model.

Intra-particle diffusion model

$$q_t = k_{\text{dif}}\, t^{0.5} + C \tag{S3}$$

Where k_{dif} (mg g^{-1} $min^{1/2}$) is the rate constant of the intra-particle diffusion model, and C (mg·g^{-1}) is the thickness of the boundary layer.

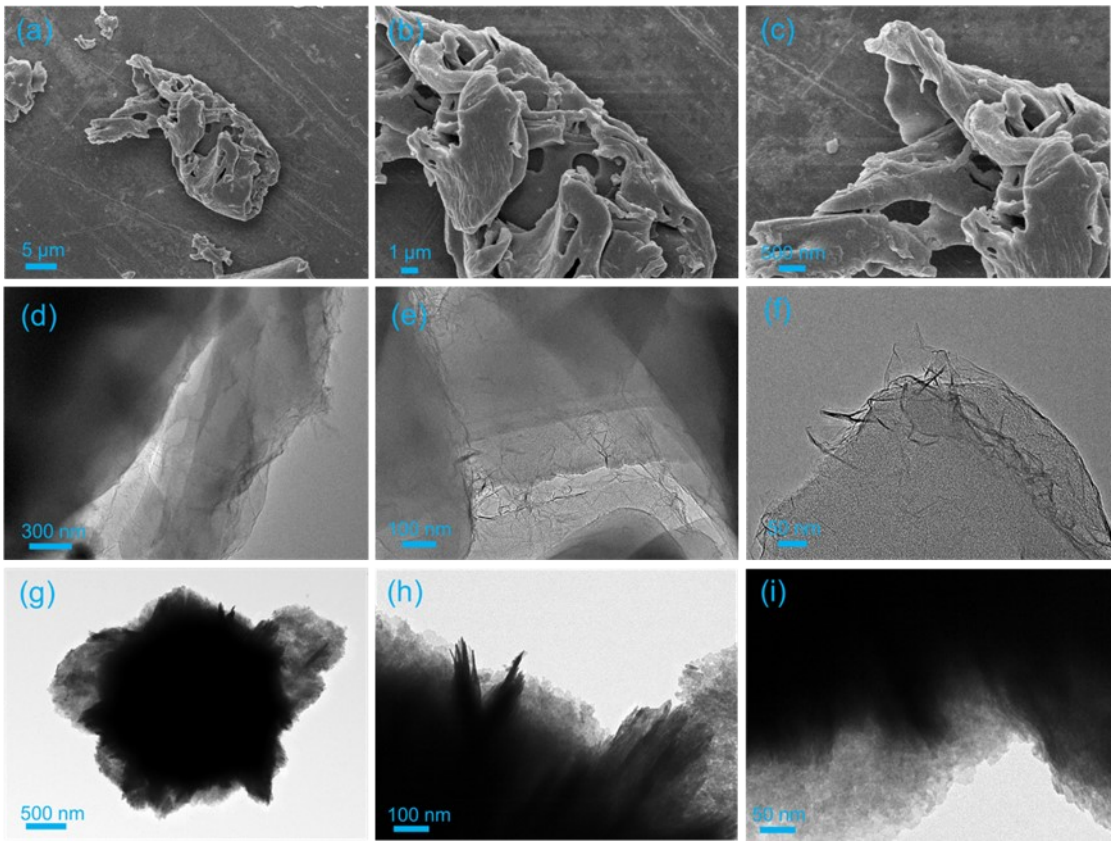

Fig. S1. (a-c) SEM images and (d-f) TEM images of BCs. (g-I) TEM images of Bi_2WO_6.

Table S1. BET surface parameters of Ni@C/ZCS samples.

Samples	Surface parameters		
	BET surface area ($m^2\ g^{-1}$)	Pore volume ($cm^3\ g^{-1}$)	Pore diameter (nm)
BiOI	15.40	0.04	34.56
Bi_2WO_6	29.64	0.08	14.13
$BWI_{0.2}$	61.69	0.18	27.64
BC	2598.30	1.21	2.38
$BC/BWI_{0.1}$	1640.73	0.94	2.55
$BC/BWI_{0.2}$	1760.00	1.04	2.60
$BC/BWI_{0.3}$	1962.42	1.15	2.57
$BC/BWI_{0.4}$	2358.99	1.37	2.49

Table S2. Kinetic parameters of BC/BWI for removal of tetracycline

Adsorbates	Samples	$q_{e,exp}$(mg g^{-1})	Pseudo-first-order model				Pseudo-second-order model			
			$q_{e,cal}$(mg g^{-1})	K_1(min^{-1})	R^2	ARE	$q_{e,cal}$(mg g^{-1})	K_2(g mg^{-1} min^{-1})	R^2	ARE
Tetracycline	BC/BW	267.27	315.52	0.089	0.994	2.86	268.20	3.51×10^{-4}	0.999	0.42
	$BC/BWI_{0.1}$	233.69	286.17	0.078	0.995	2.35	237.09	3.10×10^{-4}	0.999	0.63
	$BC/BWI_{0.2}$	227.09	271.58	0.087	0.991	3.07	229.96	3.92×10^{-4}	0.998	1.12
	$BC/BWI_{0.3}$	234.79	256.14	0.078	0.876	15.13	237.03	3.11×10^{-4}	0.999	0.52
	$BC/BWI_{0.4}$	202.59	240.22	0.090	0.992	2.96	204.24	4.70×10^{-4}	0.998	0.82

Table S3. Intra-particle diffusion parameters of BC/BWI for removal of tetracycline

Adsorbates	Samples	Intra-particle diffusion parameters							
		$k_{dif\,1}$(mg g^{-1} $min^{1/2}$)	C_1	R^2	ARE	$k_{dif\,2}$(mg g^{-1} $min^{1/2}$)	C_2	R^2	ARE
Tetracycline	BC/BW	40.96	31.72	0.971	3.94	4.43	232.63	0.976	0.14
	$BC/BWI_{0.1}$	38.28	9.24	0.994	1.56	5.29	193.60	0.878	0.47
	$BC/BWI_{0.2}$	37.63	15.28	0.996	1.99	2.91	204.59	0.999	0.01
	$BC/BWI_{0.3}$	38.95	6.87	0.989	1.75	6.61	183.98	0.981	0.22
	$BC/BWI_{0.4}$	32.54	19.72	0.994	2.77	2.53	183.14	0.989	0.07

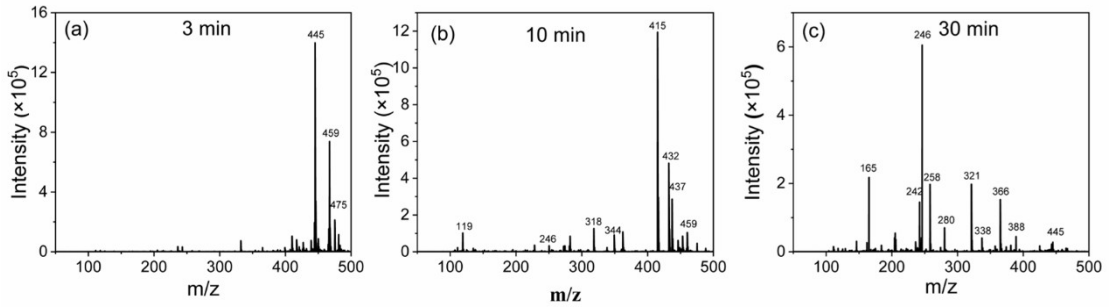

Fig. S2. (a-c) Degraded tetracycline mass spectrometry.

Table S4. Comparison of adsorption- photocatalysis capacity of tetracycline.

catalyst	pollutant	Photore-action time (min)	Catalytic dose (mg)	q_m (mg g^{-1})	light source	removal efficiency	Reference
β-cyclodextrin/Cu_2O	Tetracycline	40	25	90	Visible light	97.0 %	1
BC/g-C_3N_4	Tetracycline	600	10	130.0	45 W LED lamp	96.0 %	2
Cu-doped Bi_2O_2S	Tetracycline	30	30	1.75	Visible light	79 %	3
plasma-TiO_2	Tetracycline	10	15	/	UV-light	90.2 %	4
CdS-N/ZnO	Tetracycline	100	20	22	500 W xenon lamp	97.0 %	5
GCN-Rod	Tetracycline	360	25	/	Visible light	100.0 %	6
N-deficient g-C_3N_4	Tetracycline	60	20	/	30 W LED lamp	85.0 %	7
BiOBr/MXene/g-C_3N_4	Tetracycline	80	25	20	Visible light	99.0 %	8

FeP/Fe single	Tetracycline	30	7.5	/	Visible light	100.0 %	9
CN/In_2S_3	Tetracycline	10	25	/	Visible light	83.0 %	10
$g\text{-}C_3N_4/g\text{-}C_3N_{4-x}$	Tetracycline	60	50	/	Visible light	88.4 %	11
C_3N_5	Tetracycline	100	10	/	Visible light	73.5 %	12
In_2S_3@PCN-224	Tetracycline	40	8	/	Visible light	82.0 %	13
Cu_2O/BC	Tetracycline	120	30	/	Visible light	85.0 %	14
MIL-53(Fe)/PVDF	Tetracycline	120	20	/	Visible light	93.0 %	15
In_2O_3/AgI	Tetracycline	10	100	/	Visible light	98.4 %	16
$CdTe/Bi_2WO_6$	Tetracycline	135	50	4.8	Visible light	91.5 %	17
Fe-g-C_3N_4/Bi_2WO_6	Tetracycline	120	20	7.5	Visible light	98.42 %	18
($CQDs/Bi_2WO_6$	Tetracycline	40	1	/	Visible light	89 .0%	19

$Bi_2WO_6/CuBi_2O_4$	Tetracycline	60	50	/	Visible light	91.0 %	20
Bi_2WO_6	Tetracycline	100	50	/	Visible light	91.0 %	21
Visible light	Tetracycline	100	30	50	Visible light	95.1 %	22
$Bi_2WO_6/BiOI/g\text{-}C_3N_4$	Tetracycline	60	20	/	300 W xenon lamp	90.0 %	23
Ag-doped $Bi_2WO_6/BiOI$	Tetracycline	150	20	14.6	Visible light	96.2 %	24
$Bi_2WO_6/BiOI@Fe_3O_4$	Tetracycline	180	2.5	2.72	Visible light	97.0 %	25
BC/BWI	Tetracycline	60	10	227.09	visible light	99.8 %	This work

References

1. H. Wang, X. Quan, Q. Xiong, L. Yin, Y. Tian and J. Zhang, Enhanced performance of β-cyclodextrin modified Cu_2O nanocomposite for efficient removal of tetracycline and dyes: Synergistic role of adsorption and photocatalysis, *Appl. Sur. Sci.*, 2023, **621,** 156735.
2. H. Zhang, Y. Yu, Y. Li, L. Lin, C. Zhang, W. Zhang, L. Wang and L. Niu, A novel BC/g-C_3N_4 porous hydrogel carrier used in intimately coupled photocatalysis and

biodegradation system for efficient removal of tetracycline hydrochloride in water, *Chemosphere*, 2023, **317**, 137888.

3. Y. Xing, X. Jiang, L. Han, X. Jin, G. Ni, Y. Peng, X. Yong and X. Wang, Efficient degradation of tetracycline over vacancy-modified Cu-doped Bi_2O_2S via peroxymonosulfate activation and photocatalysis, *J. Clean. Prod.*, 2023, **400,** 136631.
4. S. Wang, Z. Zhou, R. Zhou, Z. Fang and P. J. Cullen, Highly synergistic effect for tetracycline degradation by coupling a transient spark gas–liquid discharge with TiO_2 photocatalysis, *Chem. Eng. J.*, 2022, **450,** .
5. W. Gong, X. Wei, Y. Han, S. Subhan, X. Yu, T. Ji, W. Sun, Y. Zhang, Z. Shi, Z. Zhao and Z. Zhao, Photon localization-assisted visible light photocatalysis of photonic crystal CdS-N/ZnO heterojunction for efficient photodegradation tetracycline hydrochloride, *Sep. Purif. Technol.*, 2023, **316,** 138409.
6. Z. Xu, S. Gong, W. Ji, S. Zhang, Z. Bao, Z. Zhao, Z. Wei, X. Zhong, Z.-T. Hu and J. Wang, Photocatalysis coupling hydrogen peroxide synthesis and in-situ radical transform for tetracycline degradation, *Chemical Engineering Journal*, 2022, **446,** 137009.
7. H. Sun, F. Guo, J. Pan, W. Huang, K. Wang and W. Shi, One-pot thermal polymerization route to prepare N-deficient modified g-C_3N_4 for the degradation of tetracycline by the synergistic effect of photocatalysis and persulfate-based advanced oxidation process, *Chem. Eng. J.*, 2021, **406,** 126844.
8. K. Gao, L.-a. Hou, X. An, D. Huang and Y. Yang, BiOBr/MXene/gC_3N_4 Z-

scheme heterostructure photocatalysts mediated by oxygen vacancies and MXene quantum dots for tetracycline degradation: Process, mechanism and toxicity analysis, *Appl. Catal. B: Environ.*, 2023, **323,** 122150.

9. X. Li, J. Hu, Y. Deng, T. Li, Z.-Q. Liu and Z. Wang, High stable photo-Fenton-like catalyst of FeP/Fe single atom-graphene oxide for long-term antibiotic tetracycline removal, *Appl. Catal. B: Environ.*, 2023, **324,** 122243.
10. J. Zhang, R. Balasubramanian and X. Yang, Novel 3D multi-layered carbon nitride/indium sulfide heterostructure for boosted superoxide anion radical generation and enhanced photocatalysis under visible light, *Chem. Eng. J.*, 2023, **453,** 139776.
11. C. Feng, X. Ouyang, Y. Deng, J. Wang and L. Tang, A novel g-C_3N_4/g-C_3N_{4-x} homojunction with efficient interfacial charge transfer for photocatalytic degradation of atrazine and tetracycline, *J Hazard Mater.*, 2023, **441**, 129845.
12. C. Fu, T. Wu, G. Sun, G. Yin, C. Wang, G. Ran and Q. Song, Dual-defect enhanced piezocatalytic performance of C_3N_5 for multifunctional applications, *Appl. Catal. B: Environ.*, 2023, **323,** 122196.
13. F.-Z. Chen, Y.-J. Li, M. Zhou, X.-X. Gong, Y. Gao, G. Cheng, S.-B. Ren and D.-M. Han, Smart multifunctional direct Z-scheme In_2S_3@PCN-224 heterojunction for simultaneous detection and photodegradation towards antibiotic pollutants, *Appl. Catal. B: Environ.*, 2023, **328,** 122517.
14. Z. Zhang, J. Liang, W. Zhang, M. Zhou, X. Zhu, Z. Liu, Y. Li, Z. Guan, C.-S. Lee, P. K. Wong, H. Li and Z. Jiang, Modified-pollen confined hybrid system: A

promising union for visible-light-driven photocatalytic antibiotic degradation, *Appl. Catal. B: Environ.*, 2023, **330,** 122621.

15. C.-J. Wu, I. Valerie Maggay, C.-H. Chiang, W. Chen, Y. Chang, C. Hu and A. Venault, Removal of tetracycline by a photocatalytic membrane reactor with MIL-53(Fe)/PVDF mixed-matrix membrane, *Chem. Eng. J.*, 2023, **451,** 138990.
16. J. Liu, C. Meng, X. Zhang, S. Wang, K. Duan, X. Li, Y. Hu and H. Cheng, Direct Z-scheme In_2O_3/AgI heterojunction with oxygen vacancies for efficient molecular oxygen activation and enhanced photocatalytic degradation of tetracycline, *Chem. Eng. J.*, 2023, **466,** 143319.
17. P. Yang, C. Chen, D. Wang, H. Ma, Y. Du, D. Cai, X. Zhang and Z. Wu, Kinetics, reaction pathways, and mechanism investigation for improved environmental remediation by 0D/3D CdTe/Bi_2WO_6 Z-scheme catalyst, *Appl. Catal. B: Environ.*, 2021, **285,** 119877.
18. C. Liu, H. Dai, C. Tan, Q. Pan, F. Hu and X. Peng, Photo-Fenton degradation of tetracycline over Z-scheme Fe-g-C_3N_4/Bi_2WO_6 heterojunctions: mechanism insight, degradation pathways and DFT calculation, *Appl. Catal. B: Environ.*, 2022, **310,** 121326.
19. H. Ren, F. Qi, A. Labidi, J. Zhao, H. Wang, Y. Xin, J. Luo and C. Wang, Chemically bonded carbon quantum dots/Bi_2WO_6 S-scheme heterojunction for boosted photocatalytic antibiotic degradation: Interfacial engineering and mechanism insight, *Appl. Catal. B: Environ.* 2023, **330,** 122587.
20. X. Yuan, D. Shen, Q. Zhang, H. Zou, Z. Liu and F. Peng, Z-scheme

$Bi_2WO_6/CuBi_2O_4$ heterojunction mediated by interfacial electric field for efficient visible-light photocatalytic degradation of tetracycline, *Chem. Eng. J.*, 2019, **369**, 292-301.

21. Y. Li, Y. Wu, H. Jiang and H. Wang, In situ stable growth of Bi_2WO_6 on natural hematite for efficient antibiotic wastewater purification by photocatalytic activation of peroxymonosulfate, *Chem. Eng. J.*, 2022, **446,** 136704.
22. W. Gao, G. Li, Q. Wang, L. Zhang, K. Wang, S. Pang, G. Zhang, L. Lv, X. Liu, W. Gao, L. Sun, Y. Xia, Z. Ren and P. Wang, Ultrathin porous Bi_2WO_6 with rich oxygen vacancies for promoted adsorption-photocatalytic tetracycline degradation, *Chem. Eng. J.*, 2023, **464,** 142694.
23. Y. Chu, J. Fan, R. Wang, C. Liu and X. Zheng, Preparation and immobilization of Bi_2WO_6/BiOI/g-C_3N_4 nanoparticles for the photocatalytic degradation of tetracycline and municipal waste transfer station leachate, *Sep. Purif. Technol.*, 2022, **300,** 121867.
24. X. Zheng, Y. Chu, B. Miao and J. Fan, Ag-doped Bi_2WO_6/BiOI heterojunction used as photocatalyst for the enhanced degradation of tetracycline under visible-light and biodegradability improvement, *J. Alloy. Compd.*, 2022, **893,** 162382.
25. Z. Mengting, T. A. Kurniawan, Y. Yanping, M. H. Dzarfan Othman, R. Avtar, D. Fu and G. H. Hwang, Fabrication, characterization, and application of ternary magnetic recyclable Bi_2WO_6/BiOI@Fe_3O_4 composite for photodegradation of tetracycline in aqueous solutions, *J. Environ. Manage.*, 2020, **270**, 110839.